Cellular/Molecular

Compartmentalized and Signal-Selective Gap Junctional Coupling in the Hearing Cochlea

Daniel J. Jagger and Andrew Forge
Centre for Auditory Research, UCL Ear Institute, University College London, London WC1X 8EE, United Kingdom

Gap junctional intercellular communication (GJIC) plays a major role in cochlear function. Recent evidence suggests that connexin 26 (Cx26) and Cx30 are the major constituent proteins of cochlear gap junction channels, possibly in a unique heteromeric configuration. We investigated the functional and structural properties of native cochlear gap junctions in rats, from birth to the onset of hearing [postnatal day 12 (P12)]. Confocal immunofluorescence revealed increasing Cx26 and Cx30 expression from P0 to P12. Functional GJIC was assessed by coinjection of Lucifer yellow (LY) and Neurobiotin (NBN) during whole-cell recordings in cochlear slices. At P0, there was restricted dye transfer between supporting cells around outer hair cells. Transfer was more extensive between supporting cells around inner hair cells. At P8, there was extensive transfer of both dyes between all supporting cell types. By P12, LY no longer transferred between the supporting cells immediately adjacent to hair cells but still transferred between more peripheral cells. NBN transferred freely, but it did not transfer between inner and outer pillar cells. Freeze fracture further demonstrated decreasing GJIC between inner and outer pillar cells around the onset of hearing. These data are supportive of the appearance of signal-selective gap junctions around the onset of hearing, with specific properties required to support auditory function. Furthermore, they suggest that separate medial and lateral buffering compartments exist in the hearing cochlea, which are individually dedicated to the homeostasis of inner hair cells and outer hair cells.

Key words: **cochlea; deafness; gap junction; hair cell; hearing; patch clamp**

Introduction

Gap junctions form intercellular channels that allow the passage of small metabolites and ions between adjacent cells. Gap junctional intercellular coupling (GJIC) has been implicated in roles as diverse as tissue growth and differentiation, cell signaling, and ion recycling (Evans and Martin, 2002; Wei et al., 2004). The importance of GJIC in the cochlea has been highlighted because of its disruption in several forms of nonsyndromic deafness (Kelsell et al., 1997; Petit et al., 2001; Marziano et al., 2003; Beltramello et al., 2005). It has been hypothesized that, after auditory transduction, sequestered K^+ is redistributed via a network of supporting cell gap junctions (Wangemann, 2002). Experimental evidence supporting such a system includes the observation of gap junction plaques in the connective tissue and organ of Corti (Kikuchi et al., 1995, 2000; Forge et al., 1999, 2002, 2003b) and the demonstration of extensive intercellular coupling (Santos-Sacchi, 1985, 1986, 1987; Mammano et al., 1996; Zhao and Santos-Sacchi, 1998, 2000; Forge et al., 2003a; Beltramello et al., 2005).

The primary constituent subunits of gap junctions are connexins, a family of membrane-spanning proteins. Gap junction channels are composed of two apposed connexin hexamers ("connexons"). The complexity of potential connexin pairings raises the possibility of homomeric or heteromeric connexons and homotypic or heterotypic channels (Evans and Martin, 2002). Gap junction channels with particular connexin arrangements have specific properties, which are most likely tailored to their physiological roles. There is significant overlap of connexin 26 (Cx26) and Cx30 immunofluorescence in cochlear tissue (Lautermann et al., 1998, 1999; Ahmad et al., 2003; Forge et al., 2003b; Sun et al., 2005). Immunogold labeling has suggested that Cx26 and Cx30 are equally distributed within individual gap junction plaques (Forge et al., 2003b). Coimmunoprecipitation experiments have shown oligomerization of Cx26 and Cx30 in cochlear tissue (Ahmad et al., 2003; Forge et al., 2003a; Sun et al., 2005). Together, these observations strongly support the existence of gap junction channels comprising heteromeric Cx26/Cx30 connexons in cochlear tissue. The molecular permeability of gap junctions consisting of Cx26 and Cx30 have been studied previously *in vitro* using dyes of different charge and molecular weight (MW), including Lucifer yellow (LY) (charge, –2; MW, 443 Da) and Neurobiotin (NBN) (charge, +1; MW, 287 Da). In heterologous expression systems, gap junctions between cells expressing Cx26 alone are permeable to LY and NBN (Manthey et al., 2001; Marziano et al., 2003). Gap junctions between cells expressing Cx30 alone transfer NBN but are impermeable to LY. Similarly, gap junctions between cells coexpressing Cx26 and Cx30 transfer NBN but are impermeable to LY (Marziano et al., 2003).

Received Oct. 7, 2005; revised Nov. 29, 2005; accepted Dec. 13, 2005.

This work was supported by grants from Deafness Research UK, the Wellcome Trust, and The Royal Society. We thank S. Casalotti, J. Gale, and R. Nickel for helpful comments on this manuscript.

Correspondence should be addressed to Dr. Daniel J. Jagger, Centre for Auditory Research, UCL Ear Institute, University College London, 332 Gray's Inn Road, London WC1X 8EE, UK. E-mail: d.jagger@ucl.ac.uk.

DOI:10.1523/JNEUROSCI.4278-05.2006

 0270-6474/06/261260-09$15.00/0

We studied GJIC in the organ of Corti of young rats. We used a combination of confocal immunofluorescence, dye injection in cochlear slices, and freeze fracture to undertake an analysis of (1) the molecular selectivity of cochlear gap junction channels *in situ*, providing a prediction of their connexin composition and (2) the native GJIC pathways after the onset of hearing.

Materials and Methods

Cochlear slice preparation. Slices were taken from Sprague Dawley rats at postnatal day 0 (P0), P8, and P12–P13. Rats were killed by intraperitoneal injection of sodium pentobarbitone, in accordance with the United Kingdom Animals (Scientific Procedures) Act of 1986. The developing bullae were excised, and the cochlear bones were exposed. Additional dissection was performed in cold artificial perilymph (in mM: 150 NaCl, 4 KCl, 2 $MgCl_2$, 1.3 $CaCl_2$, 8 NaH_2PO_4, 2 Na_2HPO_4, and 5 glucose, pH adjusted to 7.3 with NaOH). All chemicals were obtained from Sigma (Poole, UK) unless stated. The cochlear bone was mounted on a vibratome block using cyanoacrylate glue (Roti-Coll 1; Carl Roth, Karlsruhe, Germany). Slices were cut at 300–400 μm on a semiautomatic vibratome (Vibratome 1000+; TPI, St. Louis, MO), fitted with a razor blade (Wilkinson Sword, High Wycombe, UK). The vibratome was adjusted to allow a very slow blade advance (<0.1 mm/s).

Connexin immunofluorescence. Cochlear slices were prepared from three rats for each age group. Slices were fixed in 4% paraformaldehyde (PFA) in PBS, permeabilized (0.1% Triton X-100, at 35°C for 40 min), blocked (10% normal goat serum, at 35°C for 40 min), and then incubated with a monoclonal anti-Cx30 antibody (1:200; Zymed, San Francisco, USA) and a polyclonal anti-Cx26 antibody (1:200, gap28H; a gift from Prof. W. H. Evans, University of Wales College of Medicine, Cardiff, UK) overnight at 4°C. The antibodies have been tested previously for their specificity for Cx30 and Cx26 (Forge et al., 2003b). Primary antibodies were omitted in negative controls. To observe labeling, slices were incubated with anti-rabbit IgG conjugated to FITC (1:200; DakoCytomation, Carpinteria, CA) and anti-mouse IgG conjugated to tetramethylrhodamine isothiocyanate (TRITC) (1:200; Sigma) at 35°C for 40 min. After several washes, slices were mounted in glycerol/PBS and coverslipped. Slices were imaged using a confocal microscope, as described below for dye injections. Antibody incubations for all three age groups were performed in parallel using the same antibody concentrations, and the same confocal settings were used for all images.

Whole-cell dye injections. Slices were stored in oxygenated artificial perilymph and provided consistent whole-cell recordings for up to 4 h. They were placed in a recording chamber (~400 μl) mounted on an upright microscope (Axioskop; Zeiss, Oberkochen, Germany) and were superfused with oxygenated artificial perilymph. The flow rate (2–4 ml/min) was controlled by a peristaltic pump. To prevent movement, slices were held beneath short lengths of platinum wire. All experiments were conducted at room temperature (20–25°C). To maximize visibility within the ossified cochlear tissue, patch-clamp recordings were performed under near-infrared videomicroscopy (Jagger et al., 2000), using a CCD video camera (ICD 42E; Ikegami, Tokyo, Japan) and light from a 100 W halogen bulb filtered at 750 nm (center wavelength, ±10 nm). Using a large video monitor, cells could be identified accurately before patch formation. Epifluorescence illumination was not used during these recordings.

Dyes were injected into selected supporting cells during 10 min whole-cell patch-clamp recordings. In preliminary experiments using slices from P0 rats, 10 min was seen as sufficient time for Neurobiotin to transfer throughout the cells of Köllicker's organ. This duration was then kept constant to allow comparison between experiments. Recordings were performed using a patch-clamp amplifier (Axopatch 200B; Axon Instruments, Union City, CA) and a Digidata board (Axon Instruments) under the control of computer software (pClamp version 8; Axon Instruments). Patch pipettes were fabricated on a vertical puller (P30; Sutter Instruments, Novato, CA) from capillary glass (GC120TF-10; Harvard Apparatus, Edenbridge, UK). Pipettes were filled with a potassium chloride solution (in mM: 150 KCl, 10 NaCl, 2 $MgCl_2$, 10 HEPES, 0.5 EGTA, and 5 glucose, pH adjusted to 7.3 with KOH). In most experiments, this solution was supplemented with 0.1% LY (di-lithium salt; MW, 443 kDa; charge, −2) and 0.1% NBN (MW, 287 kDa; charge, +1; Vector Laboratories, Burlingame, CA). Pipette solutions were filtered at 0.2 μm and centrifuged to remove small insoluble particles. Pipettes had an access resistance of 2–4 MΩ, measured in artificial perilymph. Before patch formation, positive pressure applied to the pipette tip was minimized to prevent mechanical disruption of cell–cell interactions. Whole-cell input resistance was measured during 10 mV hyperpolarizing pulses (10 ms duration). Cells were held in the whole-cell configuration for 10 min before pipette detachment. Successful termination of whole-cell recordings was confirmed by the formation of a high-resistance membrane patch on retraction of the pipette. Slices were fixed immediately in 4% PFA for 20 min at room temperature. In preliminary experiments using P0 slices, there was no apparent difference in the extent of NBN transfer in which fixation time was varied between 20 and 60 min, suggesting that 20 min is a sufficient period of fixation. This minimum time was chosen to minimize the amount of time slices were kept in fixative. In some experiments, flufenamic acid (FFA) was added to the artificial perilymph to block gap junctions. FFA was made as 100 mM stock solution in dimethylsulfoxide (DMSO) and diluted to 100 μM in artificial perilymph before the experiment. DMSO applied alone at the final concentration of 0.1% did not affect input resistance or capacitance (data not shown). Capacitance values are given as means ± SEM. Comparisons were performed using paired or unpaired *t* tests (Prism version 4; GraphPad Software, San Diego, CA), with a probability level <0.05 considered significant.

Confocal microscopy. To detect NBN, slices were permeabilized (0.1% Triton X-100, at 35°C for 40 min), blocked (0.1 M L-lysine, at 35°C for 40 min), and incubated in Alexa Fluor 555-conjugated streptavidin (1:200 at 35°C for 2 h; Invitrogen, Carlsbad, CA). LY fluorescence is photobleached quickly during confocal microscopy, and its peak absorbance (428 nm) lies between the available laser lines. To overcome these limitations, LY was detected by incubating slices in anti-LY polyclonal antibody (1:200 with 10% normal goat serum, overnight at 4°C; Sigma). Slices were then incubated in anti-rabbit IgG conjugated to FITC (1:200 for 2 h at 35°C; DakoCytomation). Slices were mounted in glycerol/PBS (Citifluor; Agar Scientific, Stansted, UK) on glass slides with a ground cavity and coverslipped. Fluorescence was assessed using a scanning confocal microscope (LSM-Meta; Zeiss) equipped with a 63× (numerical aperture, 1.2) objective. The 543 nm line of a helium/neon laser excited Alexa Fluor 555 (NBN detection) or TRITC (Cx30 immunofluorescence), and emitted fluorescence was captured using a long-pass filter (560 nm). The 488 nm line of an argon laser excited FITC (for both LY detection and Cx26 immunofluorescence), and emitted fluorescence was captured using a bandpass filter (505–530 nm). Optical sections (~1 μm) were projected using computer software (Zeiss). Images were imported into Adobe Photoshop (Adobe Systems, San Jose, CA) and adjusted for optimal contrast and brightness. All images have been oriented with the medial aspect of the slice to the right-hand side for clarity. Postfixation differential interference contrast (DIC) images of slices were taken using a digital camera (Axiocam; Zeiss) mounted on an upright microscope (Axioskop 2 mot; Zeiss).

Freeze fracture. Freeze fracture was performed on the cochleae of six rats from each age group. Cochleae were fixed by direct perfusion of 2.5% glutaraldehyde in 0.1 M cacodylate buffer (pH 7.3 with 3 mM $CaCl_2$) and continued for 2 h. The organs of Corti were dissected under 0.1 M cacodylate buffer and infiltrated with 25% glycerol in 0.1 M cacodylate for a minimum of 45 min, before mounting in freeze-fracture planchettes using a yeast-in-glycerol paste and freezing by plunging into rapidly stirred propane/isopentane (4:1) cooled in liquid nitrogen. Fracturing was performed in a Balzers BAF400D apparatus (Bal-Tec, Balzers, Liechtenstein) using standard procedures (Forge et al., 2003b). Digital images of the freeze-fracture replicas, obtained with a Gatan 1000 Superscan camera attached to the electron microscope, were imported into Adobe Photoshop and adjusted for optimal contrast and brightness.

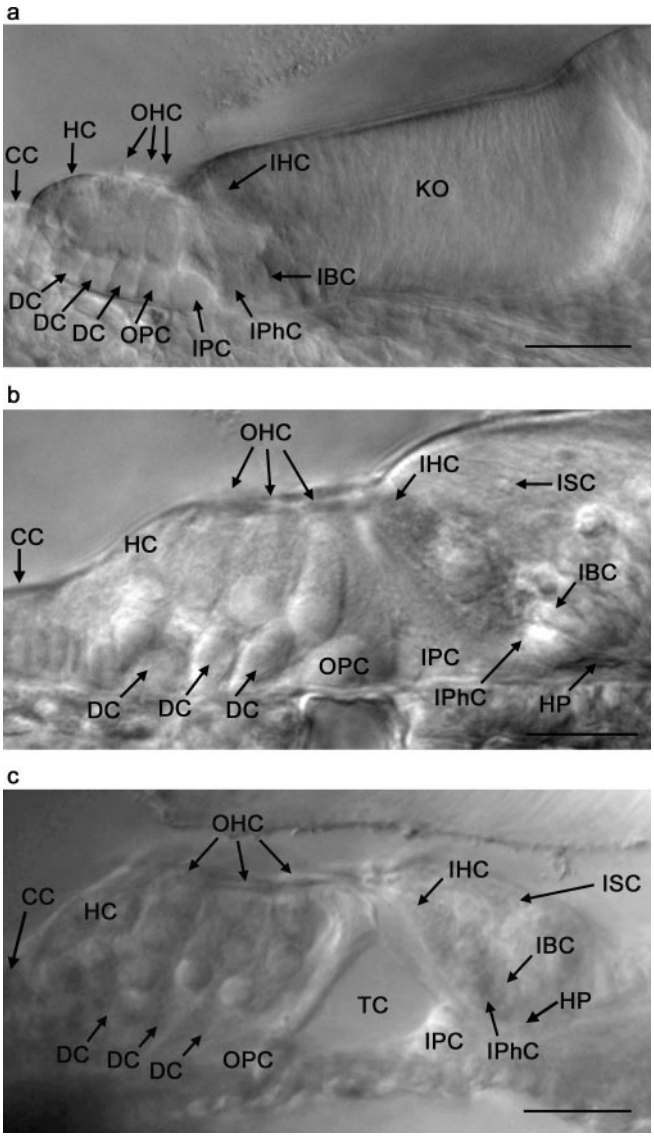

Figure 1. Postfixation DIC micrographs of the apical turn of the developing organ of Corti. ***a***, P0 organ of Corti. ***b***, P8 organ of Corti. ***c***, P13 organ of Corti. Scale bars, 20 μm. Slices shown have been used in dye transfer experiments and have been fixed, processed, and mounted for Lucifer yellow and Neurobiotin detection. CC, Claudius' cells; DC, Deiters' cell; HC, Hensen's cells; HP, habenula perforata; IBC, inner border cell; IPhC, inner phalangeal cell; IPC, inner pillar cell; ISC, inner sulcus cell; KO, Köllicker's organ; OPC, outer pillar cell; TC, tunnel of Corti.

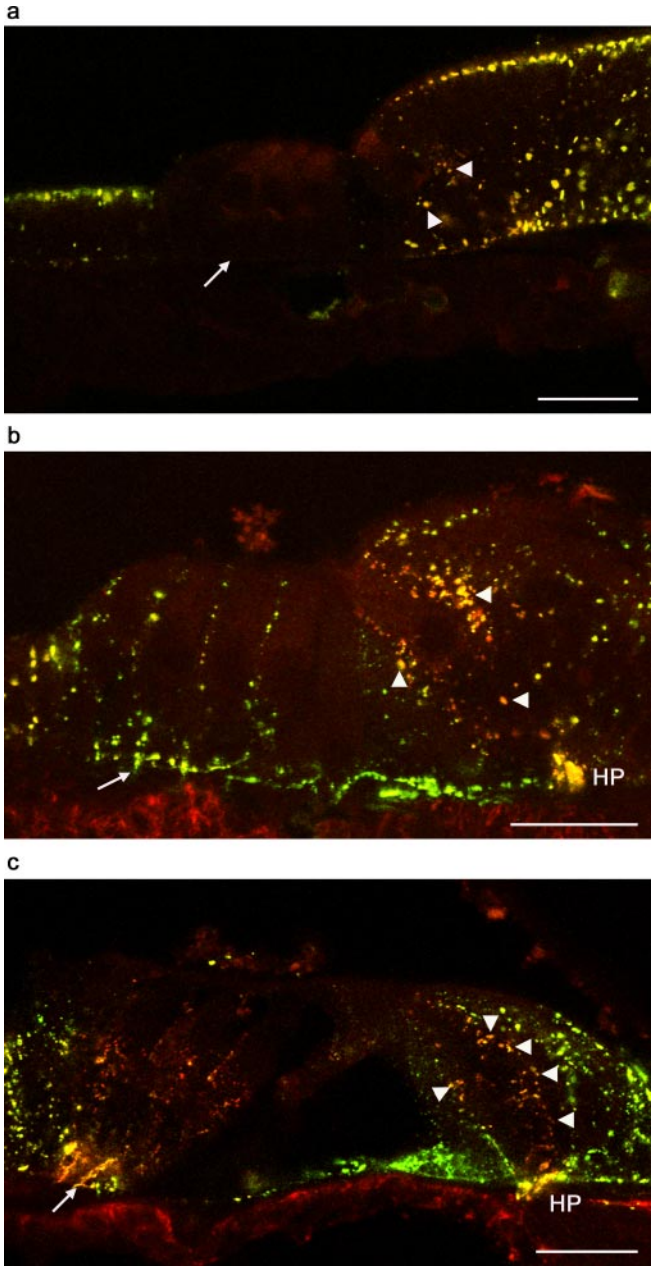

Figure 2. Localization of Cx26 and Cx30 in the apical turn organ of Corti by confocal immunofluorescence. ***a***, At P0, there was punctate colocalization of Cx26 (green) and Cx30 (red) immunofluorescence in Köllicker's organ, in the supporting cells in the medial region (around the IHC; arrowheads), and in Claudius' cells. There was no detectable immunofluorescence in the supporting cells of the lateral region (Deiters' cells, arrow, or Hensen's cells). ***b***, At P8, there was an increased immunofluorescence in all locations, including supporting cells in the medial region (arrowheads) and in the lateral region (e.g., Deiters' cells, arrow). There was noticeable colabeling in the region of the habenula perforata (HP). ***c***, At P12, there was a similar pattern of immunofluorescence but with a noticeable predominance of Cx30 in the Deiters' cells and supporting cells around IHCs (arrowheads). In Deiters' cells, the immunofluorescence of Cx26 and Cx30 was most dense near the basolateral membrane (arrow). In all peripheral supporting cells (Hensen's cells and inner sulcus cells), there was a predominance of Cx26 immunofluorescence. There was colabeling in the region of the habenula perforata (HP). Scale bars, 20 μm.

Results

Cx26 and Cx30 expression in the organ of Corti undergo extensive changes during postnatal development

Postfixation DIC micrographs of cochlear slices at P0, P8, and P13 revealed a progressive cytoarchitectural development of the organ of Corti (Fig. 1). Supporting cells separate into distinguishable regions, those medial to the tunnel of Corti, surrounding inner hair cells (IHCs), and those lateral to the tunnel, surrounding outer hair cells (OHCs). At early stages before the tunnel of Corti forms, inner pillar cells and outer pillar cells lie parallel, and both reach to the lumenal surface. With maturation, the inner pillar cell head expands over the outer pillar cell so that the outer pillar cell abuts beneath the inner pillar cell heads. At P0, the organ of Corti is compact (Fig. 1*a*). The supporting cells in the medial region, together with the greater epithelial ridge of Köllicker's organ, are continuous through to the cartilaginous spiral lamina. At P8, the tunnel of Corti has not yet begun to form in the apical turn (Fig. 1*b*), although it is partially formed in the basal turn (data not shown). By P13, the organ is noticeably less compact, with an appearance compatible with the onset of hearing function (Fig. 1*c*). In the lateral region, Deiters' cells are longer and the spaces of Nuel are formed between the OHCs and the

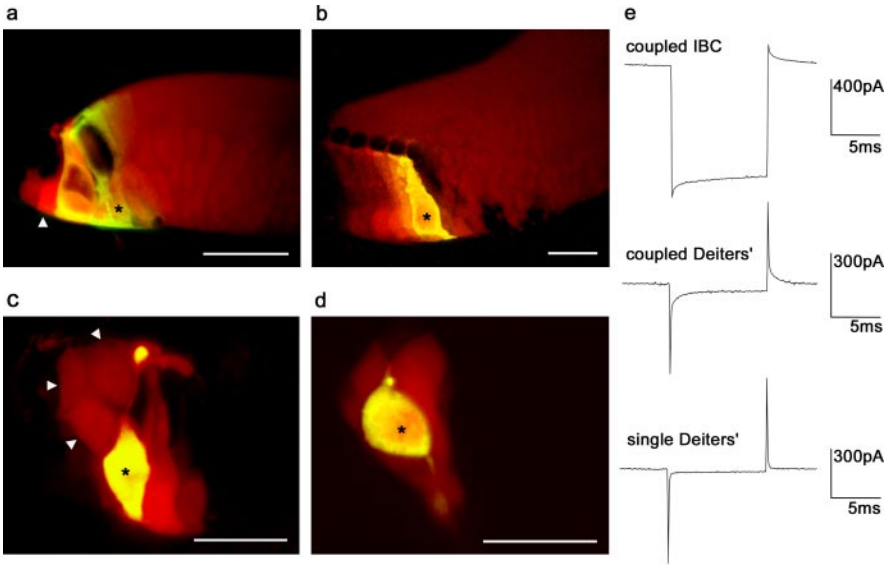

Figure 3. Nonselective GJIC in supporting cells of the P0 organ of Corti revealed by dye transfer. In all panels, an asterisk denotes the injected cell. ***a***, LY (green) and NBN (red) injected into an inner border cell during a 10 min whole-cell recording. LY spread to other supporting cells in the medial region and into cells of Köllicker's organ. NBN spread was more extensive, reaching throughout Köllicker's organ and beyond the outer pillar cell (arrowhead). Neither dye was detected in the IHC. ***b***, Injection into an inner pillar cell demonstrated longitudinal spread of NBN throughout supporting cells of the medial region and Köllicker's organ. ***c***, In the supporting cells of the lateral region, LY spread from a Deiters' cell was minimal, but NBN spread to Hensen's cells (arrowheads). ***d***, From a Hensen's cell, NBN spread to several cells, but LY spread was poor. Scale bars, 20 μm. ***e***, The input resistance and cell capacitance (estimated from the decay of the current transients) correlated well with the observed spread of NBN. Whole-cell current responses to 10 mV hyperpolarizing pulses, in a coupled inner border cell (IBC) (shown in ***a***; input resistance, 10 MΩ; decay time constant, 2.61 ms; estimated capacitance, 590 pF), a coupled Deiters' cell (shown in ***c***; 300 MΩ, 0.20 ms, 18 pF), and an uncoupled Deiters' cell displaying no NBN spread (500 MΩ, 0.06 ms, 5 pF). This cell was uncoupled at the onset of the recording and was not manipulated mechanically or pharmacologically.

outer pillar cell. The tunnel of Corti is formed in all regions, and the pillar cells have a mature rod-like appearance. Köllicker's organ is retracted, with the inner sulcus cells clearly defined.

Connexin expression in the neonatal organ of Corti was assessed using a polyclonal antibody against Cx26 and a monoclonal antibody against Cx30 (Fig. 2). There was no labeling for Cx26 or Cx30 within hair cells at any age. At all ages, there was extensive punctate colabeling of supporting cell membranes with Cx26 and Cx30 antibodies (evidenced by yellow overlay puncta), consistent with gap junction plaque localization. At P0, supporting cells in the medial region showed extensive colabeling for Cx26 and Cx30 (Fig. 2*a*). There was also extensive colabeling within the greater epithelial ridge of Köllicker's organ, particularly at the lumenal pole of the cells. There were only sparse puncta within inner pillar cells. There was strong punctate labeling for Cx26 and Cx30 in the Claudius' cells and outer sulcus cells, with highest expression in the lumenal pole. However, there was very little labeling for either Cx26 or Cx30 in the lateral region at P0. Deiters' cells and Hensen's cells were devoid of puncta.

At P8, there was coexpression of Cx26 and Cx30 between all supporting cells in the medial and lateral regions of the organ of Corti and in cells of the inner sulcus and outer sulcus (Fig. 2*b*). Labeling was seen in Claudius' cells and in the cells of the outer sulcus (data not shown). In the medial region, there was intense punctate colabeling for Cx26 and Cx30 in inner phalangeal cells (immediately lateral to IHCs), inner border cells, and inner sulcus cells. There was consistent colabeling in the region of the habenula perforata, a small opening in the bone through which dendritic nerve fibers emanate. In the lateral region, there was punctate colabeling for Cx26 and Cx30 between Hensen's cells and between Deiters' cells, with an apparent dominance of Cx26 within single puncta (revealed by a green/yellow appearance of the overlay).

By P12, there was extensive coexpression of Cx26 and Cx30 in all supporting cells in the medial and lateral regions of the organ of Corti (Fig. 2*c*). There were few examples of punctate labeling by one antibody only. In the medial region, there was punctate colabeling in the supporting cells immediately adjacent to IHCs, but more peripheral cells displayed relatively more intense Cx26 labeling (as shown by green puncta). In the lateral region, colabeled puncta were most densely concentrated in the basolateral membrane of Deiters' cells, near the basilar membrane. There appeared to be a greater contribution from Cx30 (as shown by a reddish hue in the overlay) in the apical region of Deiters' cells. Conversely, the Hensen's cells displayed relatively more intense Cx26 labeling.

Widespread postnatal changes of functional GJIC are revealed by whole-cell dye injections

We performed dye injections using whole-cell patch electrodes to investigate the molecular selectivity of native gap junctions in cochlear slices. Recordings were made from supporting cells in both the medial and lateral regions to assess the possibility of regional variations of coupling during development. There was prodigious cell–cell coupling in most whole-cell recordings. Uncoupled cells were found only occasionally and were probably the result of damage at the cut surface of slices. There were no apparent apex–base differences in coupling at any of the ages studied. Coupling was evident during the recordings from the very low input resistance (often $<$10 MΩ; equivalent to a conductance $>$100 nS), concurrent with a negative zero-current potential (V_z; typically between -40 and -80 mV). Coupling was confirmed subsequently by extensive spread of NBN (see below). The membrane capacitance (C_m) was estimated from the capacitive transients during short voltage pulses (Mammano et al., 1996). C_m was estimated as high as 925 pF (P8 slices), consistent with extensive intercellular coupling.

Analysis of NBN spread in cochlear slices at P0 revealed differences of GJIC among supporting cells in the medial (IHCs) region compared with those in the lateral (OHCs) region. A total of 13 recordings from cells in the medial region (inner phalangeal cells, inner border cells, and inner pillar cells) resulted in similar patterns of NBN and LY spread (Fig. 3*a*,*b*). NBN could be detected in all of the supporting cells around the IHCs and throughout the cells of Köllicker's organ. Notably, there was free transfer of NBN in the longitudinal plane (along the cochlear partition) (Fig. 3*b*). These recordings resulted in little NBN in the lateral region. In recordings from cells in Köllicker's organ, LY was detectable in fifth- and sixth-order cells (data not shown).

In a total of 13 recordings from cells in the lateral region (Deiters' cells, outer pillar cells, and Hensen's cells), NBN spread to surrounding cells, revealing functional coupling (Fig. 3*c*,*d*).

However, compared with injections into medial region supporting cells, this spread was poor. NBN and LY transfer was restricted to only a few cells. There was spread of NBN from Deiters' cells into Hensen's cells (Fig. 3*c*). In recordings from Hensen's cells, there was also only poor transfer of both LY and NBN (Fig. 3*d*). In all recordings at P0, the spread of NBN was more extensive than that of LY. There was no evidence for transfer of either dye into hair cells at P0. The differences in dye transfer in the medial and lateral regions were reflected in the whole-cell current responses measured during dye loading (Fig. 3*e*). In NBN-coupled recordings at P0, the estimated C_m in medial region cells (457 ± 31 pF; $n = 13$) was significantly greater than that in lateral region cells (14 ± 2 pF; $n = 13$; $p < 0.05$, unpaired *t* test) (supplemental Fig. 1, available at www.jneurosci.org as supplemental material).

At P8, recordings from supporting cells in the medial region resulted in extensive NBN spread in all directions and across to supporting cells in the lateral region (Fig. 4*a*,*b*). LY spread to several cells laterally and longitudinally. Recordings from lateral region supporting cells resulted in a similar pattern of NBN and LY spread (Fig. 4*c*,*d*), revealing an increase of GJIC compared with P0 (supplemental Fig. 1, available at www.jneurosci.org as supplemental material). There was no significant difference between the C_m of cells in the medial region (505 ± 52 pF; $n = 8$) compared with those in the lateral region (523 ± 45 pF; $n = 22$; $p > 0.05$, unpaired *t* test). There was, however, a significant increase of C_m of lateral cells at P8 compared with those at P0 ($p < 0.05$, unpaired *t* test). There was no evidence for transfer of either dye into hair cells at P8. In separate experiments in which dyes were omitted, the input resistance of coupled Deiters' cells at P8 increased during bath application of FFA (Fig. 4*e*), a putative gap junction blocker (Harks et al., 2001; Eskandari et al., 2002). The effects of FFA were first seen within 20 s and were complete within 120 s. They were essentially reversible on washout. In the presence of FFA, robust outwardly rectifying currents were revealed (Fig. 4*f*). FFA does not block the outwardly rectifying currents of isolated Deiters' cells (Jagger and Ashmore, 1998). FFA decreased C_m significantly from 503 ± 65 to 15 ± 1 pF ($n = 6$; $p < 0.05$, paired *t* test), suggesting an uncoupling of the syncitium.

By P12–P13, the distribution of NBN and LY had altered noticeably (Fig. 5). In all recordings, NBN injected into individual supporting cells transferred to other supporting cells in all directions. However, NBN did not transfer laterally from inner pillar cells to outer pillar cells (Fig. 5*a*,*b*) or medially from outer pillar cells to inner pillar cells (Fig. 5*c*,*d*). GJIC appeared to have become segregated into separate medial and lateral compartments. There was no significant difference between the C_m of supporting cells in the medial region (558 ± 78 pF; $n = 11$) compared with those in the lateral region (526 ± 41 pF; $n = 26$; $p > 0.05$, unpaired *t* test) (supplemental Fig. 1, available at www.jneurosci.org as supplemental material).

By P12–P13, there were also apparent changes in the gap junctional permeability to LY relative to earlier ages. In the medial region, in eight of eight recordings from individual supporting cells immediately adjacent to IHCs, LY did not transfer to adjacent cells (Fig. 5*a*). Similarly in the lateral region, in 13 of 13 recordings from individual Deiters' cells, LY did not transfer to any other cell (Fig. 5*c*). However, within groups of more peripheral supporting cells in both regions, LY was still able to transfer. In inner sulcus cells ($n = 3$), LY spread to adjacent similar cells but no farther (Fig. 5*b*). There was transfer of LY between Hensen's cells in 13 of 13 recordings (Fig. 5*d*), but LY did not transfer from Hensen's cells to Deiters' cells.

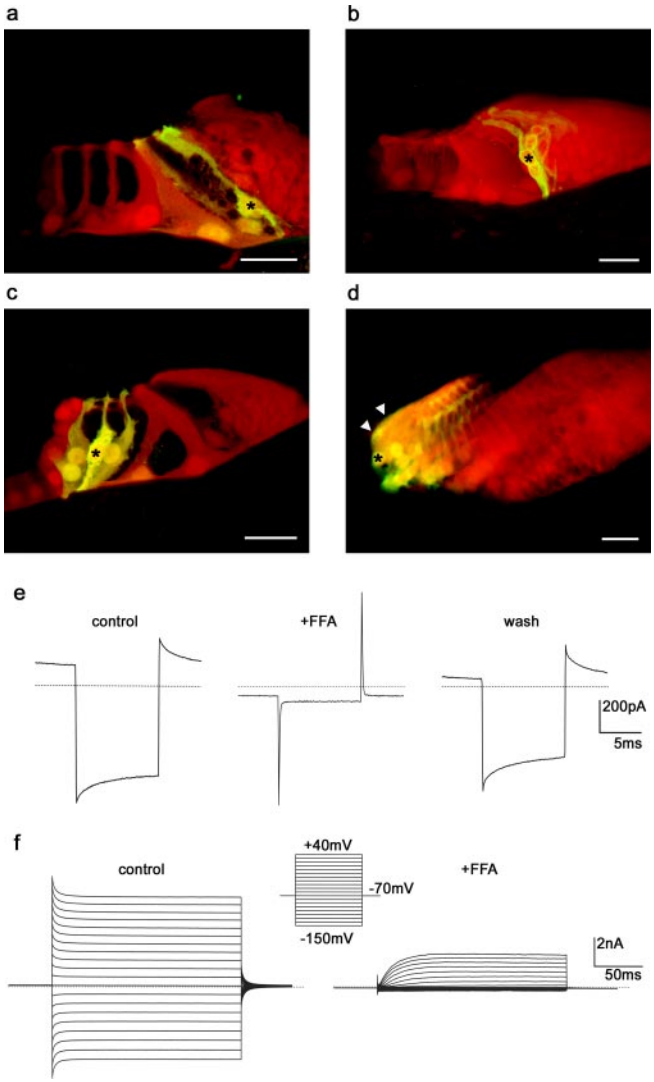

Figure 4. Nonselective GJIC persists in supporting cells of the P8 organ of Corti. In all panels, an asterisk denotes the injected cell. ***a***, LY (green) and NBN (red) injected into an inner border cell during a 10 min whole-cell recording. LY spread to other supporting cells in the medial region and into cells of Köllicker's organ. NBN spread was more extensive, reaching throughout Köllicker's organ and supporting cells in the lateral region. Neither dye was detected in the IHCs or OHCs. ***b***, There was spread of LY from an inner sulcus cell to several others and spread of NBN to all regions. ***c***, LY and NBN spread extensively (medially and laterally) from a middle row Deiters' cell. ***d***, LY spread from a Hensen's cell into other Hensen's cells (arrowheads) and Deiters' cells, and NBN transfer was extensive. Scale bars, 20 μm. ***e***, Input resistance of coupled Deiters' cells was increased reversibly by bath application of FFA (100 μM). Cell capacitance was estimated to decrease from 260 to 17 pF. Voltage pulses to −80 from −70 mV holding potential; dashed line shows zero-current level. ***f***, FFA decreased the amplitude of whole-cell currents in response to 200 ms voltage pulses (−150 to +40 mV; holding potential, −70 mV). Outwardly rectifying currents remained in the presence of FFA.

Gap junction plaque formations confirm compartmentalization of GJIC

The apparent segregation of supporting cells into distinct medial and lateral GJIC compartments was further investigated by the analysis of gap junction plaques in freeze fracture replicas of the organ of Corti. The localization and distribution of gap junctions was consistent with the patterns of NBN transfer observed at all ages. At P0 in Köllicker's organ (supplemental Fig. 2*a*, available at

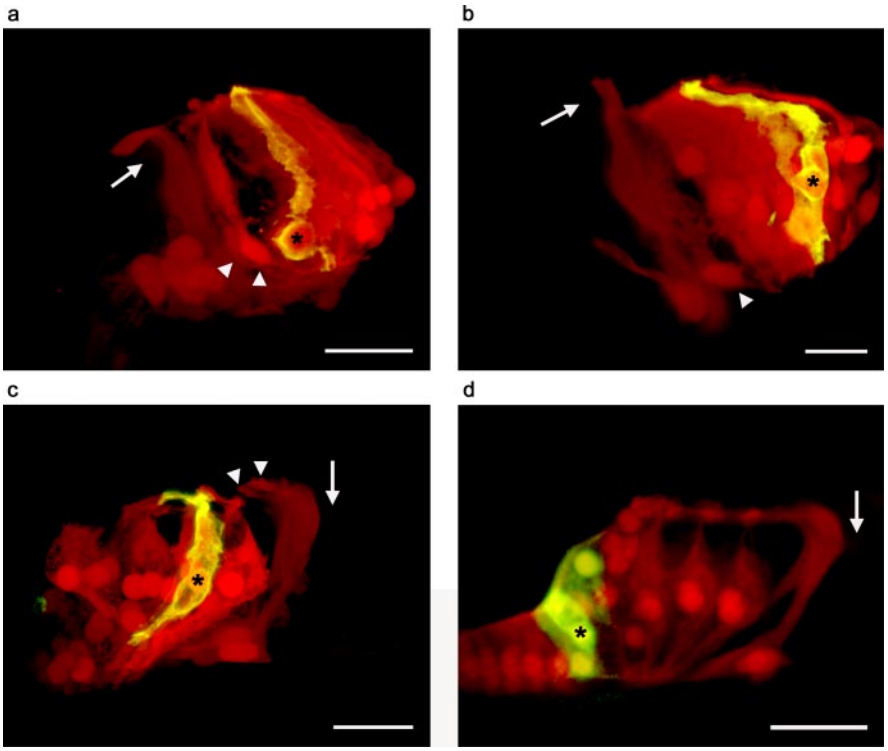

Figure 5. After the onset of hearing (P12–P13), GJIC was dye selective and compartmentalized. In all panels, an asterisk denotes the injected cell. ***a***, LY (green) and NBN (red) injected into an inner border cell during a 10 min whole-cell recording. NBN spread to all other medial region supporting cells. LY did not escape from the inner border cell to inner phalangeal cells (arrowheads). NBN did not spread laterally to the outer pillar cell (position indicated by arrow). Neither dye was detected in the IHCs. ***b***, Injection into a peripheral inner sulcus cell demonstrated LY spread to other peripheral inner sulcus cells, and NBN spread into inner phalangeal cells (arrowheads) and other medial region cells, but not into outer pillar cells (arrow). ***c***, Injection into a Deiters' cell demonstrated longitudinal spread of NBN (arrowheads) throughout the lateral region supporting cells and medially to outer pillar cells but not into inner pillar cells (arrow). LY did not escape the Deiters' cell. ***d***, Injection into a Hensen's cell demonstrated LY spread to other Hensen's cells but not into Deiters' cells. There was radial spread of NBN as far as the outer pillar cells but not into inner pillar cells (arrow). Scale bars, 20 μm.

www.jneurosci.org as supplemental material), numerous, often large gap junction plaques were present between cells at their lumenal ends just below the tight junction region (supplemental Fig. 2*b*, available at www.jneurosci.org as supplemental material), although junctions were smaller and less numerous at the basal ends of these cells (supplemental Fig. 2*c*, available at www.jneurosci.org as supplemental material). Within the organ of Corti itself, gap junction plaques were difficult to identify on the membrane fracture faces of any supporting cell type (supplemental Fig. 2*d–f*, available at www.jneurosci.org as supplemental material).

At P8, in contrast, gap junctions were clearly evident between most supporting cells (Fig. 6*a–c*). At this stage, before the opening of the tunnel of Corti when the outer pillar cells and inner pillar cells are still closely adjacent along their lateral membranes, numerous gap junction plaques were present on the membrane fracture faces between the two pillar cell types (Fig. 6*b*). This indicates the potential for intercellular communication between the medial and lateral regions. Numerous junctions between inner pillar cells and inner phalangeal cells were also evident (Fig. 6*c*). By P12, after the opening of the tunnel of Corti and the separation of the inner pillar cells and outer pillar cells along their lateral walls, gap junction plaques appeared to be absent from the remaining region of apposition in which the outer pillar cells abut beneath the expanded heads of the inner pillar cells (Fig. 6*e*). Gap junction plaques were evident, however, on the membrane faces between two adjacent outer pillar cells (Fig. 6*f*) and between the bodies of outer pillar cells and Deiters' cells (data not shown). Generally, the pattern of gap junction distribution in the organ of Corti of the rat at P12 conformed to that previously described for the mature organ of Corti in several other mammalian species (Forge et al., 2003b). For example, between the bodies of adjacent inner pillar cells in which the cells are in contact in the longitudinal direction along the organ of Corti, extremely large gap junction plaques were present (supplemental Fig. 3*a*,*b*, available at www.jneurosci.org as supplemental material). Numerous gap junctions also were present between the bodies of adjacent Deiters' cells (supplemental Fig. 3*c*,*d*, available at www.jneurosci.org as supplemental material) and were distributed in a manner identical of that observed in the mature organ of Corti.

Discussion

Our results demonstrate changes of gap junction channel characteristics and alterations in the pathways of intercellular communication in the organ of Corti during postnatal development. The characteristics of early postnatal GJIC bear little resemblance to those in the hearing cochlea. These observations have implications for the interpretation of studies of GJIC in normal hearing and disease. We have provided functional evidence for the existence of gap junction channels comprising heteromeric Cx26/Cx30 connexons in native cochlear tissue in hearing animals based on the selective transfer of diagnostic dyes, in conjunction with the colocalization of Cx26 and Cx30 within supporting cells. We found evidence for Cx26-only channels (i.e., LY permeable) only in peripheral supporting cells within the organ of Corti in hearing animals (supplemental Fig. 4, available at www.jneurosci.org as supplemental material). Furthermore, we have provided functional and anatomical evidence that is consistent with separate hypothetical K^+-recycling pathways in the cochlea. In hearing animals, there is a lateral pathway (possibly for the management of K^+) emanating from OHCs and also a novel medial pathway (for K^+) from IHCs (supplemental Figs. 4, 5, available at www.jneurosci.org as supplemental material).

The cochlear slice preparation allows the study of cochlear physiology up to and beyond the onset of hearing (Jagger et al., 2000; Jagger and Housley, 2003), when gap junction plaque formations resemble those in adult tissues and connexin expression becomes mature (Lautermann et al., 1999). There is extensive evidence for gene expression of multiple connexin subtypes early in development (Ahmad et al., 2003; Forge et al., 2003b; Cohen-Salmon et al., 2004). However, Cx26 and Cx30 are the only recognized connexin subunits present in supporting cells in the mature organ of Corti (Forge et al., 2003b). Developmental patterns of antibody labeling for Cx26 and Cx30 in the rat have been demonstrated previously (Lautermann et al., 1999) and are extended here. Because there is limited evidence for localization of

other connexin proteins in the organ of Corti, we restricted our interpretation of dye transfer in terms of Cx26- and Cx30-containing channels.

The intercellular spread of LY and NBN most likely occurred via gap junction channels. The extent and selectivity of dye transfer could be predicted by the localization of connexin protein and gap junction plaque formations. The extent of NBN spread (which would pass most gap junction channel types) was well correlated with the estimated capacitance of the syncitium, which was decreased reversibly by FFA, a broad-range gap junction blocker (Harks et al., 2001; Eskandari et al., 2002). These experiments identify FFA as a useful tool for future research into cochlear GJIC. Functional hemichannels (unmatched connexons facing the external medium) are present in the mature organ of Corti but only allow uptake of large anionic molecules under certain conditions (Zhao, 2005).

There was a progressive change in gap junction dye permeability during the first 2 postnatal weeks. We observed extensive transfer of LY at P0 and P8. Based on heterologous expression data, this can be interpreted as passage through gap junction channels comprising Cx26-only connexons (Manthey et al., 2001; Marziano et al., 2003). We observed junctional puncta predominantly labeled for Cx26 at these ages. After the onset of hearing (P12–P13), LY transfer was not evident in any recordings from supporting cells immediately adjacent to hair cells (Deiters' cells, inner border cells), suggesting a significant decrease in the numbers of Cx26-only channels between these cells in hearing animals. Because there was strong antibody colabeling for Cx26 and Cx30 in these regions, the results support the existence of channels comprising heteromeric Cx26/Cx30 connexons (Zhao and Santos-Sacchi, 2000; Ahmad et al., 2003; Forge et al., 2003b; Marziano et al., 2003; Sun et al., 2005). In more peripheral cells, such as Hensen's cells or inner sulcus cells, Cx26-only channels were evident, suggesting that there may be functionally distinct groups of supporting cells (supplemental Fig. 4, available at www.jneurosci.org as supplemental material).

The molecular selectivity of gap junctions in the organ of Corti may provide insights into their function in normal hearing and deafness. Our results show that supporting cells from hearing animals are freely permeable to small cationic molecules such as NBN (MW, 287 kDa), which may reflect K^+ flux *in vivo* (Wangemann, 2002). Transfer of the larger anion LY (MW, 443 kDa) did not occur between supporting cells immediately adjacent to hair cells, as in mature guinea pigs (Santos-Sacchi, 1986). However, because LY transfer has been observed in mature supporting cells of the chinchilla (Oberoi and Adams, 1996) and the gerbil (Zwislocki et al., 1992), interspecies and age-related differences cannot be discounted. Transfer of dye from supporting cells to hair cells (Zwislocki et al., 1992) was not seen in the present study.

Large anionic molecules such as LY and D-myo-inositol-1,4,5-trisphosphate [$Ins(1,4,5)P_3$] (MW, 420 kDa) can pass through homotypic Cx26 channels *in vitro* and through gap junctions between Hensen's cells (Beltramello et al., 2005). Our results demonstrating LY transfer in supporting cells at P0–P13 support these observations. Selective impairment of $Ins(1,4,5)P_3$ passage through homotypic Cx26-only channels is suggested to underlie certain types of recessive hereditary deafness (Beltramello et al., 2005). Our results are pertinent to the search for the causes of connexin-related deafness, because hair cell death occurs from the onset of hearing in transgenic mouse models (Cohen-Salmon et al., 2002; Kudo et al., 2003; Teubner et al., 2003). Our results suggest that, by the onset of hearing, gap junctions between supporting cells immediately adjacent to hair cells (Deiters' cells, inner border cells) do not express Cx26-only channels and so would not normally allow passage of large anions. It remains puzzling as to how connexin mutations affecting signaling between peripheral supporting cells causes extensive cochlear trauma. The role of these peripheral cells in cochlear homeostasis deserves additional study. Subtle differences between the properties of channels comprising homomeric and heteromeric connexons can influence the rate of Ca^{2+} signaling between cells (Sun et al., 2005), although it remains unclear whether Ca^{2+} signaling through heteromeric connexons is based on the intercellular transfer of $Ins(1,4,5)P_3$ and/or Ca^{2+} ions themselves. $Ins(1,4,5)P_3$ also regulates Ca^{2+} signaling in the organ of Corti in

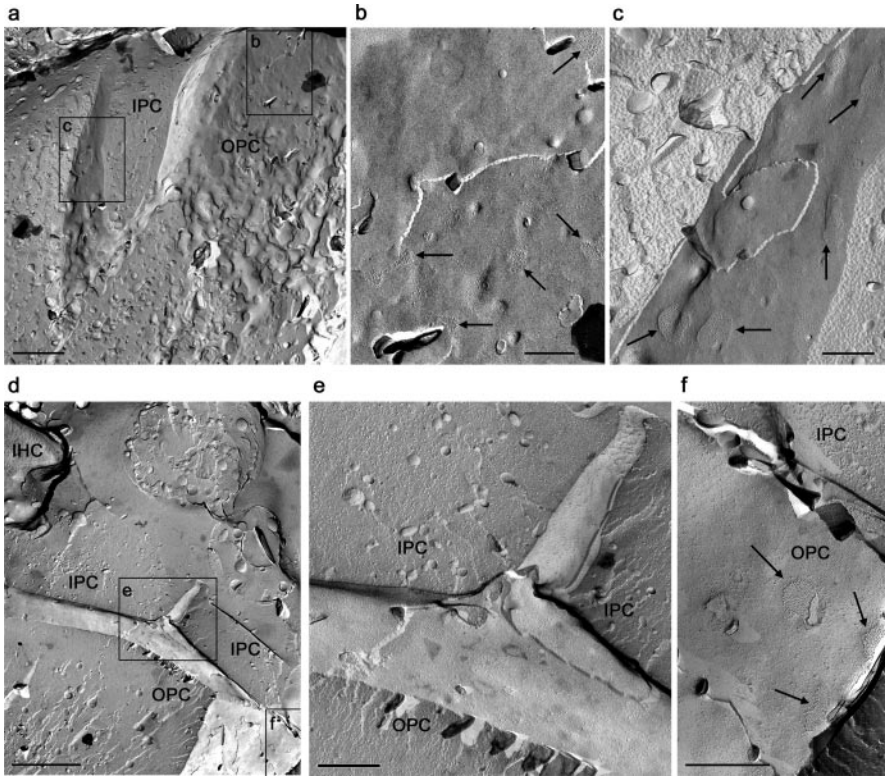

Figure 6. Freeze fracture revealed the anatomical compartmentalization of GJIC around the onset of hearing. ***a–c***, P8 organ of Corti. ***a***, Survey view of fracture across the pillar cell region revealing an inner pillar cell (IPC) adjacent to an outer pillar cell (OPC). Boxes indicate areas shown at higher power in ***b*** and ***c***. ***b***, Membrane faces of adjacent inner pillar cell and outer pillar cell show numerous gap junction plaques (arrows) down the membranes all along the regions of contact between the two cells. ***c***, Membrane face of inner pillar cell adjacent to inner phalangeal cell; numerous gap junction plaques (arrows) are exposed. ***d–f***, P12 organ of Corti. ***d***, Region in which the head of an outer pillar cell abuts below the heads of two adjacent inner pillar cells. IHC, Inner hair cell. Boxes enclose areas shown at higher power in ***e*** and ***f***. ***e***, Membrane faces in which outer pillar cells meet the heads of inner pillar cells. Gap junction plaques cannot be identified on the membrane faces in which the two cell types meet. ***f***, Membrane face of the outer pillar cell in which it is adjacent to the next outer pillar cell. Gap junction plaques (arrows) are present. Scale bars: ***a***, ***d***, 2 μm; ***b***, ***c***, ***e***, ***f***, 0.5 μm.

a GJIC-independent manner via paracrine purinergic signaling (Gale et al., 2004).

Our data from the organ of Corti at the onset of hearing point to a separate medial compartment of supporting cells that likely buffers K^+ derived from IHCs (supplemental Figs. 4, 5, available at www.jneurosci.org as supplemental material). Such a pathway has been proposed previously based on anatomical specializations and the localization of ion-transport proteins to cells of the inner sulcus and to interdental cells (Spicer and Schulte, 1998). This could provide a direct and low-resistance route for IHC-derived K^+ to scala vestibuli. In various models of deafness, particularly in models of GJIC disruption, IHCs often survive whereas OHCs are quickly lost (Cohen-Salmon et al., 2002; Kudo et al., 2003; Teubner et al., 2003). The survival of IHCs (and thus a basic level of hearing, even in the absence of the more vulnerable OHCs) may be made possible by the existence of a defined medial compartment. Also, at P0, extensive medial NBN transfer, connexin protein localization, and gap junction plaque formations demonstrate a precocious development of GJIC in this region. This is consistent with the early appearance of IHC K^+ currents compared with those in OHCs (Marcotti et al., 2004). The medial compartment may be dedicated to the protection of IHCs at all developmental stages.

Medial and lateral injections resulted in radial and longitudinal NBN transfer, demonstrating the large continuous volume of both cytoplasmic compartments. The supporting cell syncitium may act as a "sink" for excess perilymphatic K^+. Gap junction coupling could provide extensive spatial buffering, as seen in astrocytes (Leis et al., 2005) and retinal Müller cells (Karwoski et al., 1989). The widespread localization of gap junction channels, K/Cl cotransporters (Boettger et al., 2002), and aquaporins (Huang et al., 2002) could provide a passive mechanism of K^+ buffering and osmotic homeostasis. In the brain, comparable energy-independent mechanisms ensure rapid siphoning and redistribution of K^+. This prevents ionic imbalances in active regions, even during ischemic episodes (Leis et al., 2005). It remains an intriguing speculation that cochlear supporting cells use comparable dynamic mechanisms with those of reactive astrocytes, maintaining homeostasis of K^+ during periods of prolonged activity or metabolic stress.

In summary, we have shown for the first time functionally distinct medial and lateral GJIC compartments in the hearing cochlea and that, within these, there are groups of cells whose gap junctions display distinct physiological properties. Cx26/Cx30 protein expression and gap junction plaque distribution during postnatal development reflected changes of gap junction selectivity and conductance. The results are consistent with the existence of gap junction channels with varied properties, which perform cell-specific roles toward long-term cochlear homeostasis and the protection of hair cells.

References

Ahmad S, Chen S, Sun J, Lin X (2003) Connexins 26 and 30 are co-assembled to form gap junctions in the cochlea of mice. Biochem Biophys Res Commun 307:362–368.

Beltramello M, Piazza V, Bukauskas FF, Pozzan T, Mammano F (2005) Impaired permeability to Ins(1,4,5)P3 in a mutant connexin underlies recessive hereditary deafness. Nat Cell Biol 7:63–69.

Boettger T, Hubner CA, Maier H, Rust MB, Beck FX, Jentsch TJ (2002) Deafness and renal tubular acidosis in mice lacking the K-Cl co-transporter Kcc4. Nature 416:874–878.

Cohen-Salmon M, Ott T, Michel V, Hardelin JP, Perfettini I, Eybalin M, Wu T, Marcus DC, Wangemann P, Willecke K, Petit C (2002) Targeted ablation of connexin26 in the inner ear epithelial gap junction network causes hearing impairment and cell death. Curr Biol 12:1106–1111.

Cohen-Salmon M, Maxeiner S, Kruger O, Theis M, Willecke K, Petit C (2004) Expression of the connexin43- and connexin45-encoding genes in the developing and mature mouse inner ear. Cell Tissue Res 316:15–22.

Eskandari S, Zampighi GA, Leung DW, Wright EM, Loo DD (2002) Inhibition of gap junction hemichannels by chloride channel blockers. J Membr Biol 185:93–102.

Evans WH, Martin PE (2002) Gap junctions: structure and function [review]. Mol Membr Biol 19:121–136.

Forge A, Becker D, Casalotti S, Edwards J, Evans WH, Lench N, Souter M (1999) Gap junctions and connexin expression in the inner ear. Novartis Found Symp 219:134–150; discussion 151–136.

Forge A, Becker D, Casalotti S, Edwards J, Marziano N, Nickel R (2002) Connexins and gap junctions in the inner ear. Audiol Neurootol 7:141–145.

Forge A, Marziano NK, Casalotti SO, Becker DL, Jagger D (2003a) The inner ear contains heteromeric channels composed of cx26 and cx30 and deafness-related mutations in cx26 have a dominant negative effect on cx30. Cell Commun Adhes 10:341–346.

Forge A, Becker D, Casalotti S, Edwards J, Marziano N, Nevill G (2003b) Gap junctions in the inner ear: comparison of distribution patterns in different vertebrates and assessment of connexin composition in mammals. J Comp Neurol 467:207–231.

Gale JE, Piazza V, Ciubotaru CD, Mammano F (2004) A mechanism for sensing noise damage in the inner ear. Curr Biol 14:526–529.

Harks EG, de Roos AD, Peters PH, de Haan LH, Brouwer A, Ypey DL, van Zoelen EJ, Theuvenet AP (2001) Fenamates: a novel class of reversible gap junction blockers. J Pharmacol Exp Ther 298:1033–1041.

Huang D, Chen P, Chen S, Nagura M, Lim DJ, Lin X (2002) Expression patterns of aquaporins in the inner ear: evidence for concerted actions of multiple types of aquaporins to facilitate water transport in the cochlea. Hear Res 165:85–95.

Jagger DJ, Ashmore JF (1998) A potassium current in guinea-pig outer hair cells activated by ion channel blocker DCDPC. NeuroReport 9:3887–3891.

Jagger DJ, Housley GD (2003) Membrane properties of type II spiral ganglion neurones identified in a neonatal rat cochlear slice. J Physiol (Lond) 552:525–533.

Jagger DJ, Robertson D, Housley GD (2000) A technique for slicing the rat cochlea around the onset of hearing. J Neurosci Methods 104:77–86.

Karwoski CJ, Lu HK, Newman EA (1989) Spatial buffering of light-evoked potassium increases by retinal Muller (glial) cells. Science 244:578–580.

Kelsell DP, Dunlop J, Stevens HP, Lench NJ, Liang JN, Parry G, Mueller RF, Leigh IM (1997) Connexin 26 mutations in hereditary non-syndromic sensorineural deafness. Nature 387:80–83.

Kikuchi T, Kimura RS, Paul DL, Adams JC (1995) Gap junctions in the rat cochlea: immunohistochemical and ultrastructural analysis. Anat Embryol (Berl) 191:101–118.

Kikuchi T, Kimura RS, Paul DL, Takasaka T, Adams JC (2000) Gap junction systems in the mammalian cochlea. Brain Res Brain Res Rev 32:163–166.

Kudo T, Kure S, Ikeda K, Xia AP, Katori Y, Suzuki M, Kojima K, Ichinohe A, Suzuki Y, Aoki Y, Kobayashi T, Matsubara Y (2003) Transgenic expression of a dominant-negative connexin26 causes degeneration of the organ of Corti and non-syndromic deafness. Hum Mol Genet 12:995–1004.

Lautermann J, ten Cate WJ, Altenhoff P, Grummer R, Traub O, Frank H, Jahnke K, Winterhager E (1998) Expression of the gap-junction connexins 26 and 30 in the rat cochlea. Cell Tissue Res 294:415–420.

Lautermann J, Frank HG, Jahnke K, Traub O, Winterhager E (1999) Developmental expression patterns of connexin26 and -30 in the rat cochlea. Dev Genet 25:306–311.

Leis JA, Bekar LK, Walz W (2005) Potassium homeostasis in the ischemic brain. Glia 50:407–416.

Mammano F, Goodfellow SJ, Fountain E (1996) Electrophysiological properties of Hensen's cells investigated in situ. NeuroReport 7:537–542.

Manthey D, Banach K, Desplantez T, Lee CG, Kozak CA, Traub O, Weingart R, Willecke K (2001) Intracellular domains of mouse connexin26 and -30 affect diffusional and electrical properties of gap junction channels. J Membr Biol 181:137–148.

Marcotti W, Johnson SL, Kros CJ (2004) A transiently expressed SK current sustains and modulates action potential activity in immature mouse inner hair cells. J Physiol (Lond) 560:691–708.

Marziano NK, Casalotti SO, Portelli AE, Becker DL, Forge A (2003) Muta-

tions in the gene for connexin 26 (GJB2) that cause hearing loss have a dominant negative effect on connexin 30. Hum Mol Genet 12:805–812.

Oberoi P, Adams JC (1996) Intracellular transport between supporting cells of the organ of Corti. Presented at the 19th Midwinter Meeting of the Association for Research in Otolaryngology, St. Petersburg, FL, February.

Petit C, Levilliers J, Hardelin JP (2001) Molecular genetics of hearing loss. Annu Rev Genet 35:589–646.

Santos-Sacchi J (1985) The effects of cytoplasmic acidification upon electrical coupling in the organ of Corti. Hear Res 19:207–215.

Santos-Sacchi J (1986) Dye coupling in the organ of Corti. Cell Tissue Res 245:525–529.

Santos-Sacchi J (1987) Electrical coupling differs in the in vitro and in vivo organ of Corti. Hear Res 25:227–232.

Spicer SS, Schulte BA (1998) Evidence for a medial K^+ recycling pathway from inner hair cells. Hear Res 118:1–12.

Sun J, Ahmad S, Chen S, Tang W, Zhang Y, Chen P, Lin X (2005) Cochlear gap junctions coassembled from Cx26 and 30 show faster intercellular Ca^{2+} signaling than homomeric counterparts. Am J Physiol Cell Physiol 288:C613–C623.

Teubner B, Michel V, Pesch J, Lautermann J, Cohen-Salmon M, Sohl G, Jahnke K, Winterhager E, Herberhold C, Hardelin JP, Petit C, Willecke K (2003) Connexin30 (Gjb6)-deficiency causes severe hearing impairment and lack of endocochlear potential. Hum Mol Genet 12:13–21.

Wangemann P (2002) K^+ cycling and the endocochlear potential. Hear Res 165:1–9.

Wei CJ, Xu X, Lo CW (2004) Connexins and cell signaling in development and disease. Annu Rev Cell Dev Biol 20:811–838.

Zhao HB (2005) Connexin26 is responsible for anionic molecule permeability in the cochlea for intercellular signalling and metabolic communications. Eur J Neurosci 21:1859–1868.

Zhao HB, Santos-Sacchi J (1998) Effect of membrane tension on gap junctional conductance of supporting cells in Corti's organ. J Gen Physiol 112:447–455.

Zhao HB, Santos-Sacchi J (2000) Voltage gating of gap junctions in cochlear supporting cells: evidence for nonhomotypic channels. J Membr Biol 175:17–24.

Zwislocki JJ, Slepecky NB, Cefaratti LK, Smith RL (1992) Ionic coupling among cells in the organ of Corti. Hear Res 57:175–194.